ChemComm

COMMUNICATION

View Article Online
View Journal | View Issue

Cite this: *Chem. Commun.*, 2014, **50**, 11550

Received 16th May 2014,
Accepted 22nd July 2014

DOI: 10.1039/c4cc03731f

www.rsc.org/chemcomm

A bifunctional curcumin analogue for two-photon imaging and inhibiting crosslinking of amyloid beta in Alzheimer's disease†

Xueli Zhang,‡[ab] Yanli Tian,‡[ac] Peng Yuan,[d] Yuyan Li,[ab] Mohammad A. Yaseen,[a] Jaime Grutzendler,[d] Anna Moore*[a] and Chongzhao Ran*[a]

In this report, we designed a highly bright bifunctional curcumin analogue CRANAD-28. *In vivo* two-photon imaging suggested that CRANAD-28 could penetrate the blood brain barrier (BBB) and label plaques and cerebral amyloid angiopathies (CAAs). We also demonstrated that this imaging probe could inhibit the crosslinking of amyloid beta induced either by copper or by natural conditions.

An imaging probe and a drug could share a common structural scaffold and design concept considering that they have the same target.[1,2] They could also have similar interaction mechanisms and specificity requirements for the target. In traditional approaches, imaging probes and drugs are pursued separately, which are time-consuming and costly.[3,4] To overcome this disadvantage, developing agents that have potentials for therapy and imaging (theranostic) is highly desirable. Nanoparticle-based theranostics have been intensively explored;[4] however, their poor BBB penetration limits their applications in CNS diseases. Therefore, developing small molecule-based theranostics is warranted for neurodegenerative diseases such as Alzheimer's disease[2] (AD).

Amyloid beta (Aβ), a peptide of 40 or 42 amino acids, is one of the key players in AD pathology.[5] The presence of Aβ plaques is one of the hallmarks of AD.[5,6] While the degree of toxicity of amyloid plaques that contribute to the overall cognitive decline in AD remains unknown, plaques are clear sites of pathology as evidenced by the presence of dystrophic neurites and the loss of dendritic spines in their surroundings.[7,8] Furthermore, there is also some evidence that plaques may impair mitochondrial function and calcium homeostasis and lead to cell death.[9] Given these and other lines of evidence, reducing Aβ deposits and plaques remains an important aim for AD drug development.[5,10,11] Imaging probes for Aβs for both clinical and preclinical research have been reported.[10,12–15] However, small molecules that can be used both for imaging and therapy of AD are still urgently needed.[11]

Recently, we have developed curcumin analogues for detecting soluble and insoluble Aβs *in vitro*, and some of them have been successfully applied for *in vivo* near-infrared imaging in transgenic AD mice.[16–18] Based on the limited interaction mechanism of the curcumin ligands and Aβs, we also designed imidazole-containing curcumin analogues to specifically interrupt the crosslinking of Aβs that was initialized by metal ions such as copper.[19,20] However, curcumin compounds always have low quantum yield (QY), and lack theranostic properties. In this report, we designed, synthesized and tested a bifunctional compound with high brightness for two-photon imaging and potential therapy.

To overcome the low QY limitation of curcumin analogues, we hypothesized that replacing the phenyl rings with pyrazoles could increase the brightness. Conceivably, the inductive electron-withdrawing effect of one of the nitrogens of pyrazole could lead to a low tendency of electron delocalization in the system, which will decrease tautomerization of the designed compounds. It is well known that less tautomerization can reduce non-radiative decay from the excited states, thus increasing the QY.[21] On the other hand, in our previous studies,[17] we showed that imidazole containing curcumin analogues could specifically interfere with the coordination of copper with H13 and H14 (Histidine) and thus attenuate the crosslinking of Aβ. In this report, we speculated that pyrazole could also interfere with the coordination because pyrazole can coordinate with copper as well. In addition, we reasoned that phenyl substitution at the N-1 position of pyrazole could further improve the QY due to the reduction of tautomerization of pyrazole (more tautomers, more non-radiative decay).[22] Taking all the facts into consideration, CRANAD-28 was designed and synthesized (Fig. 1b).

CRANAD-28, an orange powder, was synthesized following our previously published procedures.[16,17] We first investigated its fluorescence properties such as excitation and emission, as

[a] *Molecular Imaging Laboratory, A. A. Martinos Center for Biomedical Imaging, Massachusetts General Hospital/Harvard Medical School, Building 75, Charlestown, Massachusetts 02129, USA. E-mail: cran@nmr.mgh.harvard.edu, amoore@helix.mgh.harvard.edu*
[b] *School of Pharmacy, China Pharmaceutical University, Nanjing, China*
[c] *Department of Parasitology, Zhongshan School of Medicine, Sun Yat-Sen University, Guangzhou, China*
[d] *Department of Neurology, Yale University, New Haven, CT, USA*

† Electronic supplementary information (ESI) available: Synthesis and detailed experimental procedures. See DOI: 10.1039/c4cc03731f

‡ These authors contributed equally to this work.

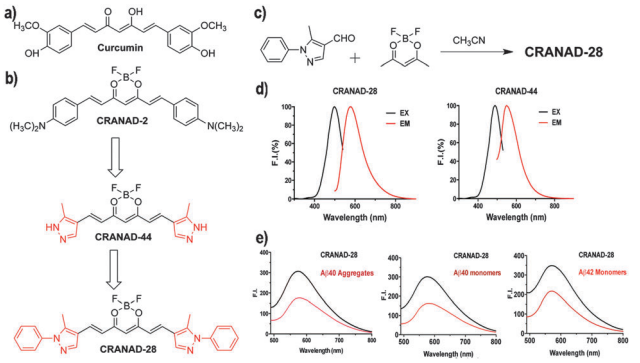

Fig. 1 (a) Structure of curcumin. (b) Design of CRANAD-28 through pyrazole replacement. (c) The synthetic route for CRANAD-28. (d) The excitation/emission spectra of CRANAD-28 and -44. (e) Fluorescence responses of CRANAD-28 with Aβ40 aggregates, Aβ40 monomers and Aβ42 monomers. For Aβ42 dimers and oligomers, the spectra are shown in Fig. S1 (ESI†).

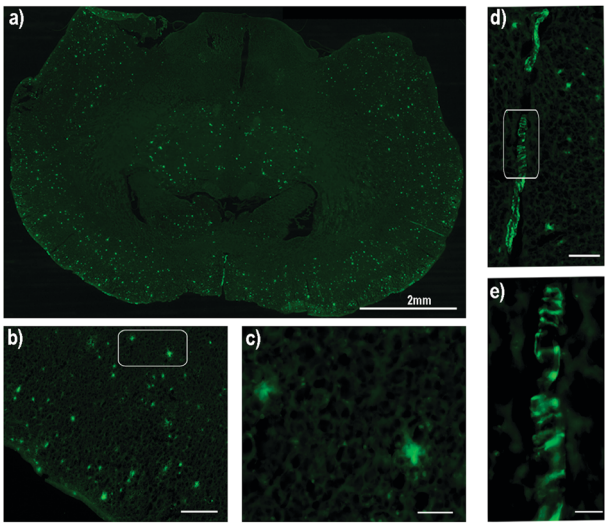

Fig. 2 Histological staining of a brain slice of an APP/PS1 mouse with CRANAD-28. (a) The image of the whole slice (2×). (b) The image of the cortex area (10×) (scale bar: 200 micron), and (c) the image of two plaques in the white box in (b) (40×) (scale bar: 100 micron). (d) The image of CAAs (10×) (scale bar: 200 micron), and (e) a magnified image of the white box in (d) (40×) (scale bar: 100 micron).

well as QY. The excitation peak of CRANAD-28 is at 498 nm and the emission peak is at 578 nm in PBS (Fig. 1d). The Stokes shift of CRANAD-28 is considerably large (80 nm), which is highly beneficial for two-photon imaging because it provides better emission penetration due to the large Stokes shift. As we expected, CRANAD-28 has a very high QY both in PBS and ethanol. The QY of CRANAD-28 is 0.32 in PBS and >1.0 in ethanol (rhodamine B was used as a reference). Our results are consistent with several references, which showed that pyrazoles are very important moieties contributing to strong fluorescence.[23–25] To confirm the N-1 phenyl substitution effect, we also synthesized CRANAD-44. As expected, the QY of CRANAD-28 was higher than that of CRANAD-44 (QY = 0.29 in PBS and 0.47 in ethanol), because the N-1 phenyl substitution can reduce the number of annular tautomers,[22] and thus reduce the non-radiative emission decay (Fig. 1b).

To test whether CRANAD-28 interacts with various Aβs, we first incubated the compound with soluble Aβs that included monomeric, dimeric, and oligomeric Aβs. We also tested the compound with insoluble Aβ40 aggregates. Interestingly, we observed that the fluorescence intensity of CRANAD-28 decreased upon mixing with all of the tested Aβs, indicating that CRANAD-28 could interact with these Aβs (Fig. 1e and Fig. S1, ESI†). The K_d values of CRANAD-28 with Aβ40 monomers, Aβ42 monomers, Aβ42 dimers, Aβ42 oligomers, and Aβ40 aggregates were 68.8, 159.7, 162.9, 85.7 and 52.4 nM, respectively (Fig. S1b, ESI†) (see details of K_d measurement in the ESI†). The intensity decrease of CRANAD-28 is contrary to our previously reported fluorescent probes, which showed an intensity increase with Aβs. No significant change was observed for CRANAD-44 with soluble Aβs (Fig. S2b and c, ESI†). The quenching mechanism for the intensity decrease of CRANAD-28 is not clear. Hintersteiner *et al.* reported that the fluorescence of imaging probe AOI987 could be slightly quenched by Aβ aggregates through an unknown mechanism,[26] and Chen *et al.* showed that Alexa fluorophores could be quenched by amino acids such as histidine, tyrosine, and methionine through static and collisional mechanisms.[27] Other mechanisms that include electron-scavenging[28] and photoinduced electron transfer (PeT)[29] were also proposed for the quenching effect induced by peptides and amino acids.[30] The fluorescence quenching of CRANAD-28 by Aβs could be due to one or a combination of the above mechanisms.

To further test whether the compounds can label Aβ plaques in AD brain tissues, we stained APP/PS1 mouse brain slices with CRANAD-28 and -44. Thioflavin S, a standard plaque-staining agent, was used for staining consecutive slices. We found that CRANAD-28 could provide an excellent contrast for Aβ plaques (Fig. 2a–c), and the distribution pattern of the highlighted plaques was similar to that obtained with thioflavin S staining. However, CRANAD-44 did not show obvious contrast for plaques, suggesting that the phenyl rings at the N-1 position could enhance the binding with Aβs (Fig. 2 and Fig. S3, ESI†). Meanwhile, CRANAD-28 not only stained the plaques, but also labeled CAAs (Fig. 2d and e), which is characterized by Aβ deposits at the exterior of the brain blood vessels that significantly contribute to pathological dementia.[31]

To investigate whether CRANAD-28 can be used for *in vivo* two-photon imaging of Aβ plaques, we firstly examined its BBB penetration. To this end, CRANAD-28 was injected i.v. into a wild type mouse, which had a surgically induced thinned skull.[32–34] We quantified the BBB penetration following the reported method,[35] and found that CRANAD-28 reached its peak around 5 minutes after injection, followed by a slow wash out (Fig. S4, ESI†). Since CRANAD-44 was not able to label Aβ plaques in the brain tissue, we didn't test BBB penetration of this compound.

Next, to validate the capability of CRANAD-28 for *in vivo* two-photon imaging of Aβ plaques, we used 9 month old APP/PS1 mice that had thinning skull surgery.[32–34] This procedure is significantly less invasive compared to cranial window preparation, which requires total removal of the skull.[36,37] In addition, it causes less damage to the neuronal cells and therefore is

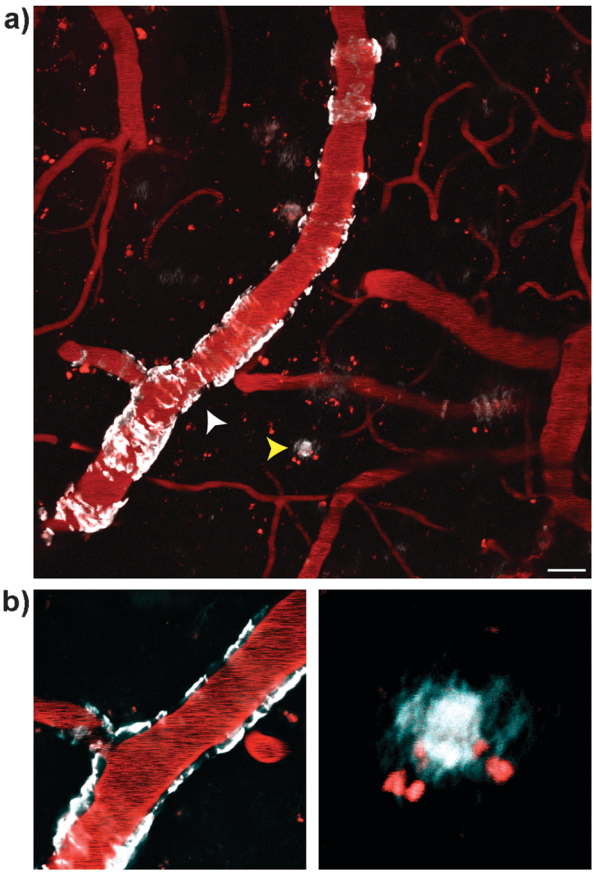

Fig. 3 Two-photon *in vivo* images of CRANAD-28 labeling in a 9 month-old APP/PS1 mouse. (a) Images were taken through a thinned-skull window 15 min after i.v. infusion of the dye. Both CAA and amyloid plaques were labeled with CRANAD-28. (b) Lower panels show zoomed-in single focal plane examples of CAA (white arrowhead, left panel) and amyloid plaques (yellow arrowhead, right panel). Blood vessels were labeled with Texas-red dextran (70 000 MW). Red punctate signals are auto-fluorescence intracellular structures. Scale bar: 25 μm.

preferable.[37] After i.v. injection of CRANAD-28, CAAs were clearly highlighted around the imaged vessels (Fig. 3a, white arrowhead). As expected, Aβ plaques could also be clearly labeled (Fig. 3a, yellow arrowhead). In Fig. 3, the blood vessels were highlighted by the injected Texas-red dextran (70 000 MW). There was a clear localization of CAAs on the walls of the vessels. These results suggested that CRANAD-28 was an effective two-photon imaging probe for both CAA and Aβ plaques. Moreover, the data also demonstrated that the longer emission of CRANAD-28 could allow for imaging to be performed with a less invasive thinning skull surgery.[32–34]

For a specific target, a non-tagged imaging probe could serve both as a ligand and a fluorophore. Conceivably, such probes could engage with the target, and thus affect the behavior of the target. For the Aβ species, CRANAD-28 could also have the capacity to change its folding/aggregating behavior, and thus to execute its anti-crosslinking effect. In our previous studies, we have demonstrated that the imidazole-containing curcumin analogue CRANAD-17 could specifically interrupt the copper induced crosslinking of Aβ, due to the imidazole moiety, which

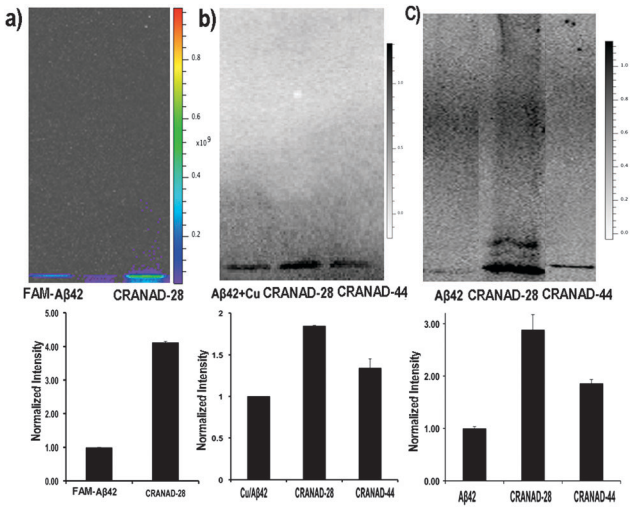

Fig. 4 Anti-crosslinking effect of CRANAD-28. (a–c) SDS-PAGE gel with FAM-Aβ42 treated with copper (a), western blotting of native Aβ42 treated with copper (b) and western blotting of native Aβ42 under natural conditions (c) (up panel). Bottom panel: quantitative analysis of the monomeric bands for each condition in the upper panel (n = 4). The normalization was based on FAM-Aβ42 treated with copper (a), Aβ42 treated with copper (b), and Aβ42 only (c).

could interfere with copper coordination with H13 and H14 of Aβ.[17] In CRANAD-28, the pyrazole ring could have the capability to coordinate with copper,[38] and thus may have the ability to compete with H13/H14 coordination. Therefore, it is reasonable to speculate that CRANAD-28 can also attenuate copper-induced crosslinking of Aβ. To this end, we first tested CRANAD-28 with FAM-Aβ42, a dye (FAM) conjugated Aβ42, to investigate the anti-crosslinking effect. As expected, there was significantly more (4.13-fold) monomeric Aβ remaining in CRANAD-28 treated samples than in the control samples, indicating reduced cross-linking (Fig. 4a). To further investigate whether it can inhibit the crosslinking of native Aβ42, we used western blotting to quantify the remaining Aβ monomers. Similar to the result obtained with FAM-Aβ42, CRANAD-28 treatment resulted in considerably more monomeric Aβ free of crosslinking (1.85-fold) (Fig. 4b).

Besides induction by metal ions, crosslinking of Aβ42 can occur naturally in solution, which is also an important factor contributing to its toxicity. To investigate whether CRANAD-28 can attenuate the natural crosslinking, we incubated it with Aβ42 in PBS buffer for 24 hours. Western blotting analysis showed that CRANAD-28 could significantly inhibit natural crosslinking of Aβ42 (2.89-fold higher than the control) (Fig. 4c).

To investigate whether the Aβ-specificity of compounds has any effect on anti-crosslinking induced by copper and a natural condition, we compared the monomeric bands of CRANAD-28 and CRANAD-44 on western blotting, and found that CRANAD-44 was not efficient in inhibiting the crosslinking of Aβ42 under both conditions (Fig. 4b and c). This is consistent with our fluorescence studies and histological staining, which indicated that CRANAD-44 was not Aβ-specific.

In summary, we demonstrated that CRANAD-28 can be considered a theranostic agent due to its imaging and potential

therapeutic functions. Through replacement of the phenyl rings with pyrazole, the resulting CRANAD-28 displayed high QY in PBS and ethanol. Previously, analogues of PiB, styrylbenzene, and other compounds have been reported to be very reliable imaging probes for two-photon imaging.[35,39,40] However, due to their short emission wavelengths, these dyes are associated with poor tissue penetrating capacities. Conceivably, CRANAD-28 has better tissue penetration because of its longer emission. The multi-color time-stamp strategy has been considered to be a very useful tool to investigate the growth kinetics of plaques, and this technique can provide a comprehensive toxicity profile of plaques.[8] We believe that fluorescent dyes with longer emissions, like CRANAD-28, can be very useful for sequential multi-color labeling to avoid *ex vivo* section staining. In addition, CRANAD-28 is not only useful for two-photon imaging but also has the capacity to attenuate crosslinking of Aβ42 induced by metal ions and natural conditions. We believe that its bifunction could contribute to AD diagnosis and therapy development in the future.

This work was supported by the K25AG036760 award to C.R. and the K99AG042026 award to M.A.Y. The authors would also like to thank Pamela Pantazopoulos, B.S. for proofreading this manuscript.

References

1 S. Vallabhajosula, *Molecular imaging: radiopharmaceuticals for PET and SPECT*, Springer-Verlag, Berlin, New York, 2009.
2 S. Aulic, M. L. Bolognesi and G. Legname, *Int. J. Cell Biol.*, 2013, **2013**, 150952.
3 A. de la Zerda, J. W. Kim, E. I. Galanzha, S. S. Gambhir and V. P. Zharov, *Contrast Media Mol. Imaging*, 2011, **6**, 346–369.
4 J. Xie, S. Lee and X. Chen, *Adv. Drug Delivery Rev.*, 2010, **62**, 1064–1079.
5 D. J. Selkoe, *Nat. Med.*, 2011, **17**, 1060–1065.
6 C. L. Joachim, H. Mori and D. J. Selkoe, *Nature*, 1989, **341**, 226–230.
7 J. Tsai, J. Grutzendler, K. Duff and W. B. Gan, *Nat. Neurosci.*, 2004, **7**, 1181–1183.
8 C. Condello, A. Schain and J. Grutzendler, *Sci. Rep.*, 2011, **1**, 19.
9 H. Xie, J. Guan, L. A. Borrelli, J. Xu, A. Serrano-Pozo and B. J. Bacskai, *J. Neurosci.*, 2013, **33**, 17042–17051.
10 R. Jakob-Roetne and H. Jacobsen, *Angew. Chem.*, 2009, **48**, 3030–3059.
11 W. Yang, Y. Wong, O. T. Ng, L. P. Bai, D. W. Kwong, Y. Ke, Z. H. Jiang, H. W. Li, K. K. Yung and M. S. Wong, *Angew. Chem.*, 2012, **51**, 1804–1810.
12 M. Ono, H. Watanabe, H. Kimura and H. Saji, *ACS Chem. Neurosci.*, 2012, **3**, 319–324.
13 M. Cui, M. Ono, H. Watanabe, H. Kimura, B. Liu and H. Saji, *J. Am. Chem. Soc.*, 2014, **136**, 3388–3394.
14 N. P. Cook, M. Ozbil, C. Katsampes, R. Prabhakar and A. A. Marti, *J. Am. Chem. Soc.*, 2013, **135**, 10810–10816.
15 C. Ran, W. Zhao, R. D. Moir and A. Moore, *PLoS One*, 2011, **6**, e19362.
16 C. Ran, X. Xu, S. B. Raymond, B. J. Ferrara, K. Neal, B. J. Bacskai, Z. Medarova and A. Moore, *J. Am. Chem. Soc.*, 2009, **131**, 15257–15261.
17 X. Zhang, Y. Tian, Z. Li, X. Tian, H. Sun, H. Liu, A. Moore and C. Ran, *J. Am. Chem. Soc.*, 2013, **135**, 16397–16409.
18 C. Ran and A. Moore, *Mol. Imaging Biol.*, 2012, **14**, 293–300.
19 C. S. Atwood, G. Perry, H. Zeng, Y. Kato, W. D. Jones, K. Q. Ling, X. Huang, R. D. Moir, D. Wang, L. M. Sayre, M. A. Smith, S. G. Chen and A. I. Bush, *Biochemistry*, 2004, **43**, 560–568.
20 G. Thiabaud, S. Pizzocaro, R. Garcia-Serres, J. M. Latour, E. Monzani and L. Casella, *Angew. Chem.*, 2013, **52**, 8041–8044.
21 J. Lakowicz, *Principles of Fluorescence Spectroscopy*, Plenum Publishing Corporation, 2nd edn, 1999.
22 J. de Paz, J. Elguero, C. Foces-Foces, A. Llamas-Saiz, F. Aguilar-Parrilla, O. Klein and H. Limbach, *J. Chem. Soc., Perkin Trans. 2*, 1997, 101–109.
23 W. Song, Y. Wang, J. Qu, M. M. Madden and Q. Lin, *Angew. Chem.*, 2008, **47**, 2832–2835.
24 Z. Yu, L. Y. Ho and Q. Lin, *J. Am. Chem. Soc.*, 2011, **133**, 11912–11915.
25 T. Ren, H. Cheng, J. Zhang, W. Li, J. Guo and L. Yang, *J. Fluoresc.*, 2012, **22**, 201–212.
26 M. Hintersteiner, A. Enz, P. Frey, A. L. Jaton, W. Kinzy, R. Kneuer, U. Neumann, M. Rudin, M. Staufenbiel, M. Stoeckli, K. H. Wiederhold and H. U. Gremlich, *Nat. Biotechnol.*, 2005, **23**, 577–583.
27 H. Chen, S. S. Ahsan, M. B. Santiago-Berrios, H. D. Abruna and W. W. Webb, *J. Am. Chem. Soc.*, 2010, **132**, 7244–7245.
28 M. R. Eftink and C. A. Ghiron, *Anal. Biochem.*, 1981, **114**, 199–227.
29 G. Bottari, G. de la Torre, D. M. Guldi and T. Torres, *Chem. Rev.*, 2010, **110**, 6768–6816.
30 M. Sauer and H. Neuweiler, *Methods Mol. Biol.*, 2014, **1076**, 597–615.
31 E. E. Smith and S. M. Greenberg, *Stroke*, 2009, **40**, 2601–2606.
32 J. Grutzendler, N. Kasthuri and W. B. Gan, *Nature*, 2002, **420**, 812–816.
33 J. Grutzendler, G. Yang, F. Pan, C. N. Parkhurst and W. B. Gan, *Cold Spring Harb Protoc.*, 2011, **2011**, pdb.prot065474.
34 D. F. Marker, M. E. Tremblay, S. M. Lu, A. K. Majewska and H. A. Gelbard, *JoVE*, 2010, e2059.
35 B. J. Bacskai, G. A. Hickey, J. Skoch, S. T. Kajdasz, Y. Wang, G. F. Huang, C. A. Mathis, W. E. Klunk and B. T. Hyman, *Proc. Natl. Acad. Sci. U. S. A.*, 2003, **100**, 12462–12467.
36 R. Mostany and C. Portera-Cailliau, *JoVE*, 2008, e680.
37 H. T. Xu, F. Pan, G. Yang and W. B. Gan, *Nat. Neurosci.*, 2007, **10**, 549–551.
38 T. Otieno, J. Blanton, M. Hatfield, S. Asher and S. Parkin, *Acta Crystallogr., Sect. C: Cryst. Struct. Commun.*, 2002, **58**, m182–m185.
39 E. E. Nesterov, J. Skoch, B. T. Hyman, W. E. Klunk, B. J. Bacskai and T. M. Swager, *Angew. Chem.*, 2005, **44**, 5452–5456.
40 Z. Liu, C. Condello, A. Schain, R. Harb and J. Grutzendler, *J. Neurosci.*, 2010, **30**, 17091–17101.